



# Stabilization of hexachloride net with mixed Sn(IV) metal complex and 2,3-dimethylanilinium organic cation: elaboration, optical, spectroscopic, computational studies and thermal analysis

Souhir Bel Haj Salah<sup>1</sup> · Sabrine Hermi<sup>1</sup> · Abdullah A. Alotaibi<sup>2</sup> · Khalid M. Alotaibi<sup>3</sup> · Frédéric Lefebvre<sup>4</sup> · Werner Kaminsky<sup>5</sup> · Cherif Ben Nasr<sup>1</sup> · Mohamed Habib Mrad<sup>1,2</sup>

Received: 22 June 2021 / Accepted: 3 November 2021 / Published online: 28 January 2022  
© Institute of Chemistry, Slovak Academy of Sciences 2021

## Abstract

A new  $(C_8H_{12}N)_2SnCl_6 \cdot 2H_2O$  was isolated from a slow evaporation reaction at ambient temperature. The title compound crystallizes in the triclinic/ $P\bar{1}$  space group, as determined by X-ray diffraction (XRD). The anions  $[SnCl_6]^{2-}$  and the  $H_2O$  molecules are connected via O–H...Cl H-bonds to build up inorganic sheets extending on the plane ( $a, b$ ) at  $z=0$  and the  $(C_8H_{12}N)^+$  cations are inserted between two successive layers and connect them through multiple H-bonds to make an infinite 3D structure. The intermolecular interactions were fully characterized using the Hirshfeld surface analysis, while the associated 2D fingerprints plots were generated to understand their contribution in building the solid-state architecture within the structure. Powder XRD was used to verify the purity of the crystalline sample phase. FT-IR and CP-MAS  $^{13}C$  NMR spectroscopy were used to investigate the vibrational modes and NMR characteristics. Moreover, the optical properties were investigated. The DFT calculations were utilized to explain these findings and determine the gap energy using the HOMO and LUMO energies. In addition, the XPS analysis was reported to analyze the surface chemistry. Finally, the thermal analysis by TG/DTA were performed, to determine its thermal behavior.

**Keywords** Sn(IV) complex · X-ray diffraction · Enrichment ratio · FT-IR spectroscopy · Optical property · XPS · DFT calculations

## Introduction

In the chemistry field, the synthesis of new functional materials has focused on inorganic–organic materials due to their interesting structural features and the advantages of

assembling their properties in a single compound with stable physico-chemical performances (Chouaib et al. 2015; Visbal and Gimeno 2014; Masternak et al. 2016; Era et al. 1994; Kagan et al. 1999). The inorganic part provides a high carrier density and mobility, as well as thermal stability, while the organic component exhibits excellent optical characteristics and potential conductivity (Bujak and Zaleski 2001; Karoui et al. 2012). Thus, the hybrid compound can be applied in several fields such as catalysis, magnetism, optic and luminescence (Vishwakarma et al. 2011; Fonseca et al. 2005; Zdanowska-Fraczek et al. 2009; Hajlaoui et al. 2013; Mathlouthi et al. 2017). Due to the dielectric confinement effect, halostannates(IV) hybrid materials exhibit remarkable exciton binding energies and substantial optical and electroluminescence capabilities (Pradesh et al. 2010; Plowas et al. 2011; Hajlaoui et al. 2013; Mrad et al. 2019; Adhikari et al. 2016). For the organic entities, we focused on systems containing  $\pi$ -conjugate systems. Due to their broad range of uses, these materials have attracted significant attention. Aniline and its derivatives, such as 2,3-dimethylaniline, represent one of the most important classes of  $\pi$ -conjugated

✉ Mohamed Habib Mrad  
m.mrad@su.edu.sa

<sup>1</sup> Present Address: Laboratoire de Chimie des Matériaux, Faculté des Sciences de Bizerte, Université de Carthage, 7021 Zarzouna, Tunisie

<sup>2</sup> Department of Chemistry, College of Sciences and Humanities, Shaqra University, Ad-Dawadmi 1191, Kingdom of Saudi Arabia

<sup>3</sup> Department of Chemistry, College of Science, King Saud University, Riyadh, Kingdom of Saudi Arabia

<sup>4</sup> Laboratoire de Chimie Organométallique de Surface (LCOMS), Ecole Supérieure de Chimie Physique Electronique, 69626 Villeurbanne Cedex, France

<sup>5</sup> Department of Chemistry, University of Washington Seattle, Washington, USA

molecules. Furthermore, the addition of substituent group to aniline affects the molecule's charge distribution, influencing its structural, electronic and vibrational characteristics (Vaschetto et al. 1999). To show the potential application of this compound, we compare our compound with similar compound based also on aniline; 2,6-dimethylanilium hexachlorostannate (IV). Indeed, this latter was screened for antibacterial activity against some bacterial strains such as *Escherichia coli* and *Salmonella typhimurium*. The antibacterial tests revealed that this compound is efficacious against the tested bacteria, inhibiting them to different degrees but significantly. This inhibitory effect on the growth of these micro-organisms is most likely owing to the blockage of their active sites. Furthermore, for such compounds, the AC conductivity measurements reveal a hopping conduction process (Mathlouthi et al. 2017). Our objective was to create a novel organic–inorganic salt based on 2,3-dimethylaniline that may find use in the area of materials science in future. Here, we provide a great understanding of the relationship between the synthesis, crystal structures and the properties such as optical and the thermal behavior. Furthermore, the theoretical analysis by Hirshfeld surface was reported, allowing us to discuss the strength of hydrogen bonds and to quantify the inter-contacts in the crystal packing. The DFT calculations, moreover was used to correlate the experimental and theoretical results.

## Experimental

### Synthesis of $(C_8H_{12}N)_2SnCl_6 \cdot 2H_2O$

Single crystals of  $(C_8H_{12}N)_2SnCl_6 \cdot 2H_2O$  were developed, at room temperature, by acid–base response between  $SnCl_4$  ( $10^{-3}$  mmol), 2,3-dimethylaniline and hydrochloric acid (10 mL). The mixture was well blended for 45 min and after that kept at room temperature. After two weeks, colorless prismatic monocrystals of very high quality showed up solution (yield: 75%).

### Investigation techniques

At room temperature, the PXRD pattern was recorded on a Siemens D5000 powder diffractometer using  $Cu-K\alpha$  radiation with  $2\theta$  within the extend 5–50°. The XRD data were acquired using a Bruker APEX-2 diffractometer equipped with a CCD area detector containing graphite monochromatized  $Mo-K\alpha$ . The Lorentz polarization and absorption effects on the intensities were taken into account (Blessing 1995). Direct techniques using the SHELXL-97 suite of programs (Sheldrick 2008) were used to distinguish the structure, then full-matrix least-squares methods were used to improve it. All calculations were performed using

SHELXL-97 in WinGX programs (Sheldrick 1997; Farrugia 1999). Diamond 2.0 (Brandenburg 1998) and Mercury 3.8 (Macrae et al. 2006) were used to create the drawings. Crystal Explorer 17.5 software was used to visualize and explore the structure's intermolecular close interactions (Turner et al. 2017). Experimental information and the structure's main geometrical features are presented in Tables 1 and 2, respectively.

The CP-MAS  $^{13}C$  NMR spectrum was measured using a Bruker DSX-500 spectrometer furnished by cross-polarization from protons and a magic angle spinning with a chemical shift given relative to tetramethylsilane (0.5 ppm precision). The Fourier transform infrared spectrum was measured on 1000-Perkin-Elmer FT-IR spectrometer. The UV absorption spectrum was measured in the range 200–800 nm with the help of Perkin-Elmer–Lambda 11UV-Vis spectrophotometer. The PL spectrum was measured utilizing Edinburgh FLSP-920 spectrofluorimeter. The XPS data was extracted from *K*-alpha Thermo instrument.

The thermal analyses (TG/DTA) were made with a TGA-Q500-TA instrument utilizing nitrogen gas.

**Table 1** Experimental details

<i>Crystal data</i>	
Chemical formula	$2(C_8H_{12}N) Sn Cl_6 \cdot 2(H_2O)$
$M_r$	611.79
Crystal system, space group	Triclinic, $P\bar{1}$
Temperature (K)	293
a, b, c (Å)	7.152 (5), 7.704 (5), 11.237 (5)
$\alpha, \beta, \gamma$ (°)	94.316 (5), 92.311 (5), 91.506 (5)
$V$ (Å <sup>3</sup> )	616.6 (6)
$Z$	1
Radiation type	$MoK\alpha$
$\mu$ (mm <sup>-1</sup> )	1.7
Crystal size (mm)	0.51 × 0.22 × 0.17
<i>Data collection</i>	
Diffractometer	Bruker APEX-II
Absorption correction	Multi-scan
$T_{min}, T_{max}$	0.46, 0.771
No. of measured, independent and observed [ $I > 2\sigma(I)$ ] reflections	17,569, 3810, 2272
$R_{int}$	0.100
$(\sin\theta/\lambda)_{max}$ (Å <sup>-1</sup> )	0.734
Refinement	
$R[F^2 > 2\sigma(F^2)], wR(F^2), S$	0.065, 0.099, 1.01
No. of reflections	3810
No. of parameters	138
No. of restraints	8
$\Delta\rho_{max}, \Delta\rho_{min}$ (e Å <sup>-3</sup> )	0.61, -0.53
CCDC No	1,578,232

**Table 2** Selected bond distances and angles in  $(C_8H_{12}N)_2SnCl_6 \cdot 2H_2O$ 

Distances (Å) in $[SnCl_6]^{2-}$			
Sn–Cl2 <sup>i</sup>	2.4232 (16)	Sn–Cl1 <sup>i</sup>	2.4236 (18)
Sn–Cl2	2.4232 (16)	Sn–Cl3 <sup>i</sup>	2.4444 (14)
Sn–Cl1	2.4237 (18)	Sn–Cl3	2.4444 (14)
Angles (°) in $[SnCl_6]^{2-}$			
Cl2 <sup>i</sup> –Sn–Cl1	89.43 (5)	Cl1–Sn–Cl3 <sup>i</sup>	90.25 (5)
Cl2–Sn–Cl1	90.57 (5)	Cl1 <sup>i</sup> –Sn–Cl3 <sup>i</sup>	89.75 (5)
Cl2 <sup>i</sup> –Sn–Cl1 <sup>i</sup>	90.57 (5)	Cl2 <sup>i</sup> –Sn–Cl3	90.00 (5)
Cl2–Sn–Cl1 <sup>i</sup>	89.43 (5)	Cl2–Sn–Cl3	90.00 (5)
Cl2 <sup>i</sup> –Sn–Cl3 <sup>i</sup>	90.00 (5)	Cl1–Sn–Cl3	89.75 (5)
Cl2–Sn–Cl3 <sup>i</sup>	90.00 (5)	Cl1 <sup>i</sup> –Sn–Cl3	90.25 (5)
Cl2 <sup>i</sup> –Sn1–Cl2	180	Cl1 <sup>i</sup> –Sn1–Cl1	180
Cl3 <sup>i</sup> –Sn1–Cl3	180.00 (5)		
Distances (Å) in $(C_8H_{12}N)^+$			
N1–C2	1.478 (5)	C1–C7	1.512 (6)
C2–C3	1.379 (6)	C5–C4	1.364 (7)
C2–C1	1.383 (6)	C5–C6	1.383 (7)
C1–C6	1.397 (7)	C6–C8	1.508 (7)
C3–C4		1.377 (7)	
Angles (°) in $(C_8H_{12}N)^+$			
C3–C2–C1	123.7 (4)	C4–C5–C6	122.5 (5)
C3–C2–N1	117.7 (4)	C5–C6–C1	118.5 (5)
C1–C2–N1	118.6 (4)	C5–C6–C8	120.0 (5)
C2–C1–C6	117.7 (4)	C1–C6–C8	121.5 (5)
C2–C1–C7	121.4 (4)	C4–C3–C2	117.5 (5)
C6–C1–C7	120.7 (4)	C5–C4–C3	120.1 (5)

Transformations codes: (i)  $-x+3, -y+1, -z+2$

## Computational details

The calculations were made utilizing the B3LYP/6-31 + G\* basis set for all atoms but the LanL2DZ pseudopotential was taken for tin using the Gaussian 09 program. The system used for the calculations contained the cation and the anion, as within the asymmetric unit. Calculations were also made on the isolated cations and anions but they did not lead to UV–visible results in agreement with experiment (peaks only at low values of  $\lambda$ ). Before calculating the different characteristics, the location of the hydrogen atoms were adjusted.

## Results and discussion

### Powder X-ray diffraction patterns

To affirm the purity of the synthesized material, the PXRD, recorded at room temperature, were contrasted with the pattern obtained from the single crystal data. It is well observed from Fig. 1, that they are indistinguishable.

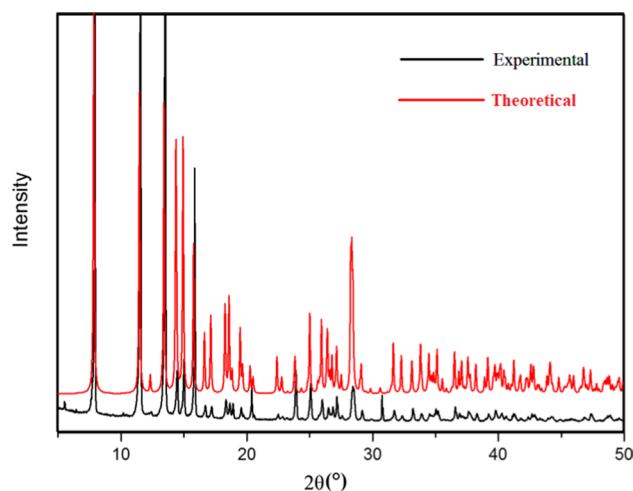


**Fig. 1** Simulated and experimental powder XRD patterns of  $(C_8H_{12}N)_2SnCl_6 \cdot 2H_2O$

### Crystal structure description

Figure 2 shows the asymmetric unit of  $(C_8H_{12}N)_2SnCl_6 \cdot 2H_2O$  and it contains one 2,3-dimethylanilinium cation, a  $H_2O$  and half of  $[SnCl_6]^{2-}$  anion, where the tin atom is located on a center of inversion. It is worth noting that, all the H atoms of the water molecule and the ammonium group are disordered (occupancy: 0.5/0.5). The atomic arrangement can be depicted as sheets parallel to the  $(a, b)$  plane at  $z=0$ , shaped by  $[SnCl_6]^{2-}$  anions and  $H_2O$  interconnected by O–H...Cl H-bonds. Additionally, the organic cations are embedded between these layers and linked them through N–H...Cl and N–H...O H-bonds (Table 3) generating an endless 3D network (Fig. 3). The stability of the crystal is improved by two kinds of interactions; the C–H... $\pi$  interactions with a distance H... $\pi$  equal to 3.293 (3) Å (Fig. 4a) (Ringer et al. 2006) and Cl...Cl interaction with a distance  $d_{Cl...Cl}$  between chlorine atoms is equal to 3.489 Å (Fig. S1) (Ouerghi et al 2018). Moreover, the interactions between the different entities in this structure are guaranteed by four sorts of hydrogen bonds, giving rise to several cycles of varying degrees  $R^2_1$  (4),  $R^5_4$  (16) and  $R^2_4$  (8) (Fig. 4b).

The 2,3-dimethylanilinium cations, trapped between two successive inorganic sheets, are arranged anti-parallel and form sheets parallel to the plane  $(a, b)$  (Fig. S2). The geometrical characteristics of these entities show a regular spatial configuration similar to other mixtures containing the same organic cation (Table 2) (Amri et al. 2008; Smirani and Rzaigui 2009). Furthermore, the water molecules play a major part in the process of ensuring the cohesion in the structure by O–H...Cl H-bonds. Figure S3 shows that the water molecules are arranged in pairs around the inversion centers at  $(0, 0, 0)$ . The geometric characteristics of the water molecule are as follows: a distance between

**Fig. 2** The ORTEP representation (the atoms-numbering scheme and displacement ellipsoids drawn at 50% probability level)

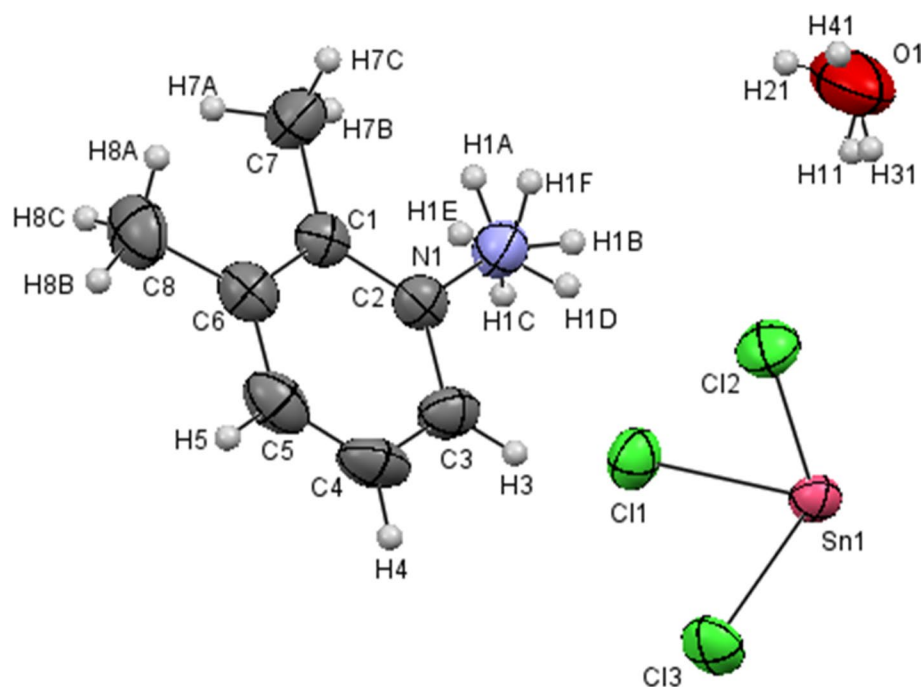


**Table 3** Hydrogen-bond geometry (Å, °)

D–H...A	<i>d</i> (D–H)	<i>d</i> (H...A)	<i>d</i> (D...A)	∠(DHA)
N(1)–H(1F)...O(1) <sup>ii</sup>	0.89	1.92	2.785 (6)	164.9
N(1)–H(1B)...Cl(2)	0.89	2.62	3.405 (5)	147.3
N(1)–H(1D)...Cl(1)	0.89	2.58	3.347 (4)	145.1
N(1)–H(1E)...Cl(3) <sup>iii</sup>	0.89	2.43	3.298 (4)	165.1
N(1)–H(1E)...Cl(1) <sup>iv</sup>	0.89	2.97	3.390 (4)	111.1
O(1)–H(11)...Cl(3) <sup>i</sup>	0.79 (2)	2.87 (4)	3.558 (5)	146 (4)
O(1)–H(11)...Cl(2)	0.79 (2)	2.80 (2)	3.446 (5)	140 (4)
O(1)–H(21)...O(1) <sup>iii</sup>	0.79 (2)	2.34 (9)	3.069 (10)	153 (17)
O(1)–H(41)...Cl(1) <sup>v</sup>	0.80 (2)	2.83 (4)	3.615 (5)	169 (15)

Transformations codes: (i)  $-x+3, -y+1, -z+2$  (ii)  $-x+2, -y, -z+2$  (iii)  $x-1, y, z$  (iv)  $-x+2, -y+1, -z+2$  (v)  $x, y-1, z$

the oxygen atom O1 and the two hydrogen atoms H11 and H21 equal to 0.850 (10) Å and an angle to 107.7 (4)° (greater than 104.5°). This value can be explained with the engagement of the water molecules in different hydrogen bonds type of different strengths (Table 3).

Globally, the whole geometry is created through a reversal center where tin lying on a special position at (½, ½, 0) crystallographic position. The [SnCl<sub>6</sub>]<sup>2-</sup> anions have a distorted octahedral geometry. To estimate the distortion, the bond length and bond angle distortion indices were calculated with the Baur distortion indices (ID) (Baur 1974) using Eqs. (1) and (2):

$$ID(\text{Sn} - \text{Cl}) = \sum_{i=1}^{n1} \frac{|d_i - dm|}{n1dm} \quad (1)$$

$$ID(\text{Cl} - \text{Sn} - \text{Cl}) = \sum_{i=1}^{n2} \frac{|a_i - am|}{n2am} \quad (2)$$

The values of the distortion indices are 0.333 for the bond length distortion and 0.252 for the bond angle distortion indices. This proves that the coordination geometry around the metal is slightly deformed. These values are in full concurrence with comparative compounds (Shahzadi et al. 2008; Feddaoui et al. 2019; Chouaib et al. 2016; Saber et al. 2017).

Comparing the crystallographic characteristics of (C<sub>8</sub>H<sub>12</sub>N)<sub>2</sub>SnCl<sub>6</sub>·2H<sub>2</sub>O (I) (Table 1) and those of (C<sub>8</sub>H<sub>12</sub>N)<sub>4</sub>[BiBr<sub>6</sub>]<sub>2</sub>NO<sub>3</sub>·2H<sub>2</sub>O (II) (Aloui et al. 2015). The space group, unit cell characteristics, and atomic layouts are the primary differences between them. In fact, for compound (II) they are: *a* = 25.8217 (1) Å, *b* = 7.8909 (2) Å, *c* = 21.4328 (3) Å with *Z* = 4 and *V* = 4367.07 (13) Å<sup>3</sup>. It appears that the inorganic part made with [BiBr<sub>6</sub>]<sup>3-</sup> and [NO<sub>3</sub>]<sup>-</sup> anions do expand the volume of the cell also the crystal system and space group which goes from the triclinic P  $\bar{1}$  for compound (I) to the orthorhombic Pca<sub>21</sub> for compound (II). It is worth mentioning that these differences influence basically the atomic arrangement and the framework of hydrogen bonds. The crystal structure of (II) is built up with alternating inorganic and organic layers and held together through N–H...Br and N–H...O(W) hydrogen bonds. Moreover, the hydrogen bonds of

**Fig. 3** Projection along the *a*-axis of the crystal packing

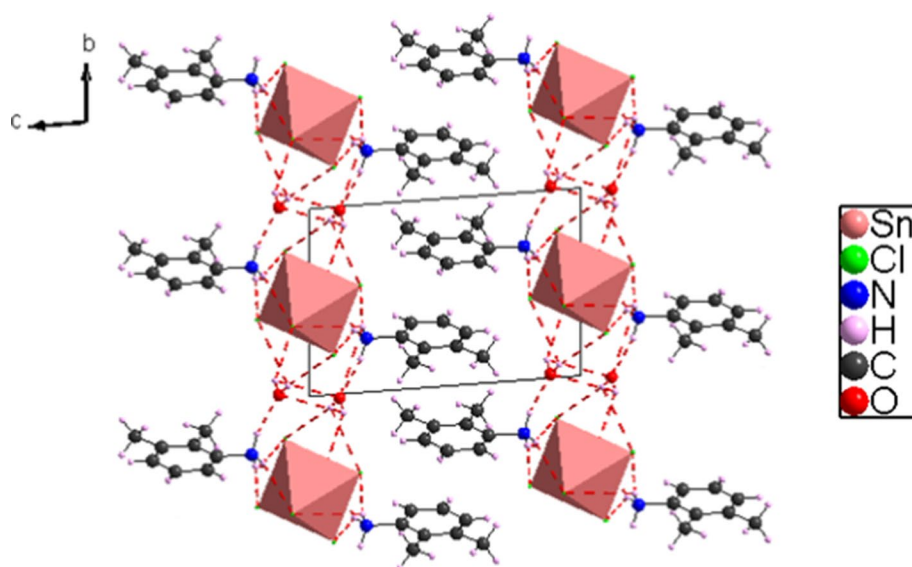
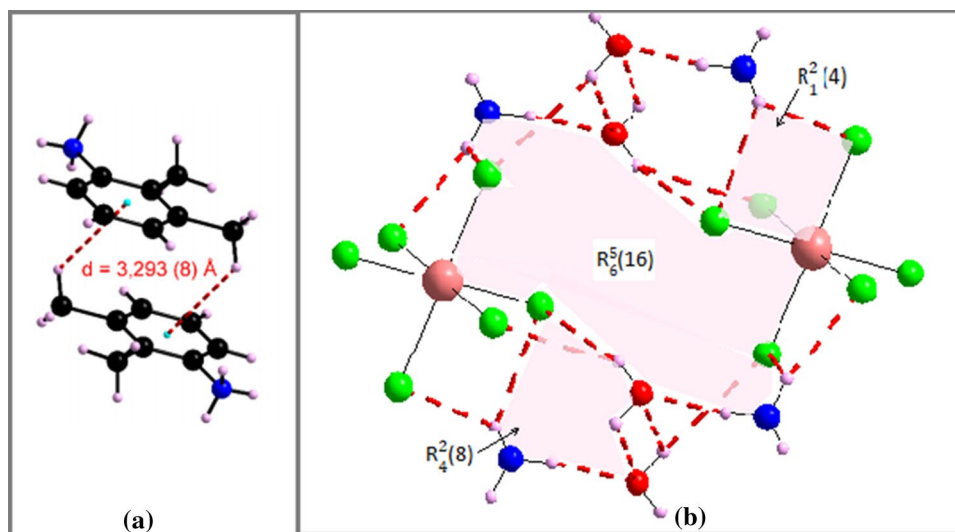


**Fig. 4** C–H... $\pi$  interactions between two neighboring cations (a). Anion-cation-cater types hydrogen bond units (b). For figure clarity only one position of the disordered hydrogen atoms is considered



type O–H...O between H<sub>2</sub>O molecules and NO<sub>3</sub><sup>−</sup> ions add more stability to the crystal packing. Both of the compounds (I) and (II) are settled by multiple hydrogen bonds and the electrostatic association adds more stability and union the 3D network.

### Hirshfeld surface analysis

The HS gives a three-dimensional picture for the asymmetric unit, known as dnorm, of the intermolecular interaction (Fig. 5) (Spackman and Jayatilaka 2009; McKinnon et al. 2004). The related two-dimensional unique fingerprint maps were drawn to measure the contacts in

this compound and it was utilized to highlight specific atom pairs in close contact (Khanam et al. 2015; Ma et al. 2015; Kumar et al. 2013). Figure 6a depicts the contributions from various kinds of interactions that cover the whole fingerprint. The enrichment ratio  $E_{XY}$  for a given combination of chemical components (*X*, *Y*) is characterized as the ratio between  $C_{XY}$  (the percentage of actual contact) and  $R_{XY}$  (the equidistributed contact) (Table 4).

The H...Cl contacts are the most noteworthy encountered interaction and are outlined in Fig. 6b by a pair of sharp spikes typical of strong H-bonding. Their contribution reaches 37.8%. In fact, these kinds of contact is the most common interaction due to the plenitude

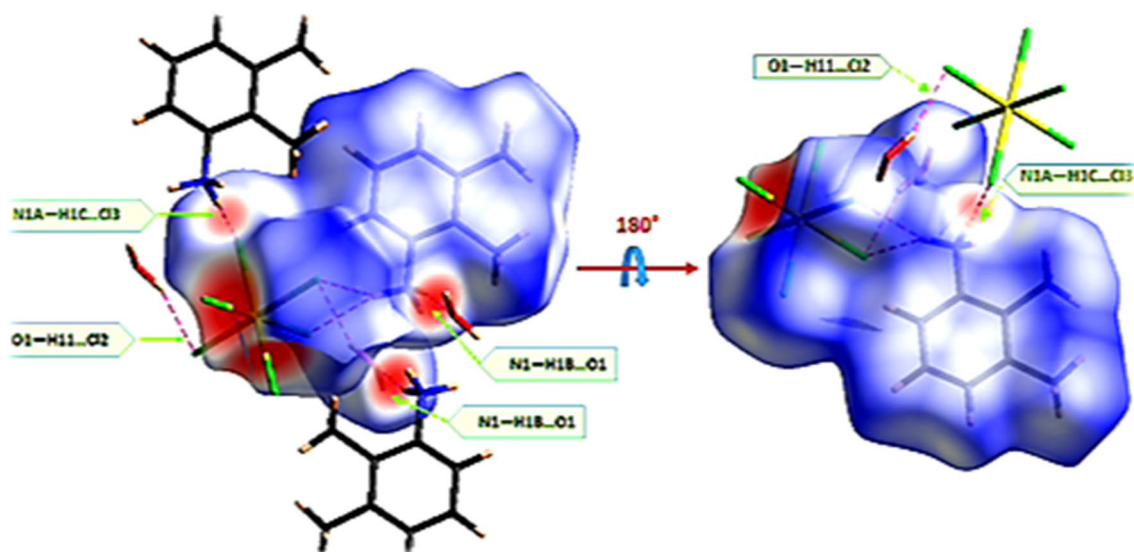


Fig. 5 View of the  $d_{\text{norm}}$  mapped in the Hirshfeld surface

of chloride and hydrogen on the molecular surface ( $\%S_{\text{H}} = 59.75\%$ ;  $\%S_{\text{Cl}} = 25.05\%$ ) and  $E_{\text{Cl}\dots\text{H}}$  reaches 1.263 (Table 4). Then, the second most common contact is the H...H contacts involving 33.6% of the whole Hirshfeld surface and show up as an expansive region with a high concentration within the center region on the 2D fingerprint map (Fig. 6c). The C...H contact represents 7.8% of the entire Hirshfeld surface (Fig. 6d) and an enrichment ratio  $E_{\text{C}\dots\text{H}} = 0.894$ . Followed by O...H, which refers to N–H...O and O–H...O contact, representing 6.7% as shown in Fig. 6e and an enrichment ratio higher than the unit (1.674) (Table 4). The Sn...Cl contact contribute 6.1% to the total area (Fig. 6f). In fact, the  $[\text{SnCl}_6]^{2-}$  octahedral also contributes to the molecular surface and displays an enrichment value  $E_{\text{Sn}\dots\text{Cl}} = 3.99$ . In addition, the C...C contact contributes only by 3.4% to the whole surface area, but more enriched  $E_{\text{C}\dots\text{C}} = 6.38$ , this sort of contact corresponds to  $\pi$ - $\pi$  interaction and due to the stacking between aromatic rings (Fig. 6g) and followed by the Cl...Cl contact representing 3.1% (Fig. 6h). Thereby, the Hirshfeld surface analysis affirms the presence of the Cl...Cl interaction discussed in the crystal description.

### Quantum mechanical study

Figure 7 illustrates that the highest occupied orbital (HOMO) is found on the hexachlorostannate anion, whereas the lowest unoccupied orbital (LUMO) is basically found on the organic cation. Furthermore, the band gap, defined as  $t$  a basic parameter in determining the

compound's stabilization, is found to be equal to 3.73 eV which implies a high kinetic stability and low chemical reactivity (Fig. S4).

### Molecular electrostatic potential MEP analysis

The MEP maps plays a key part within the recognizable proof of active sites within the chemical holding of new chemicals. This analysis is utilized to estimate the atomic and electronic charge scattering of the molecule. As appeared in Fig. 8, the positive and negative zones are being located on the organic cation.

### Mulliken population

The Mulliken population technique is a significantly fruitful method of recognizing nucleophilic or electrophilic attacks and the sensitive regions to other molecular interactions. The Mulliken charge distributions of all atoms, gotten with the same methodology as above, are given in Table S1. The atoms of  $(\text{C}_8\text{H}_{11}\text{N})$  are numbered as follows:

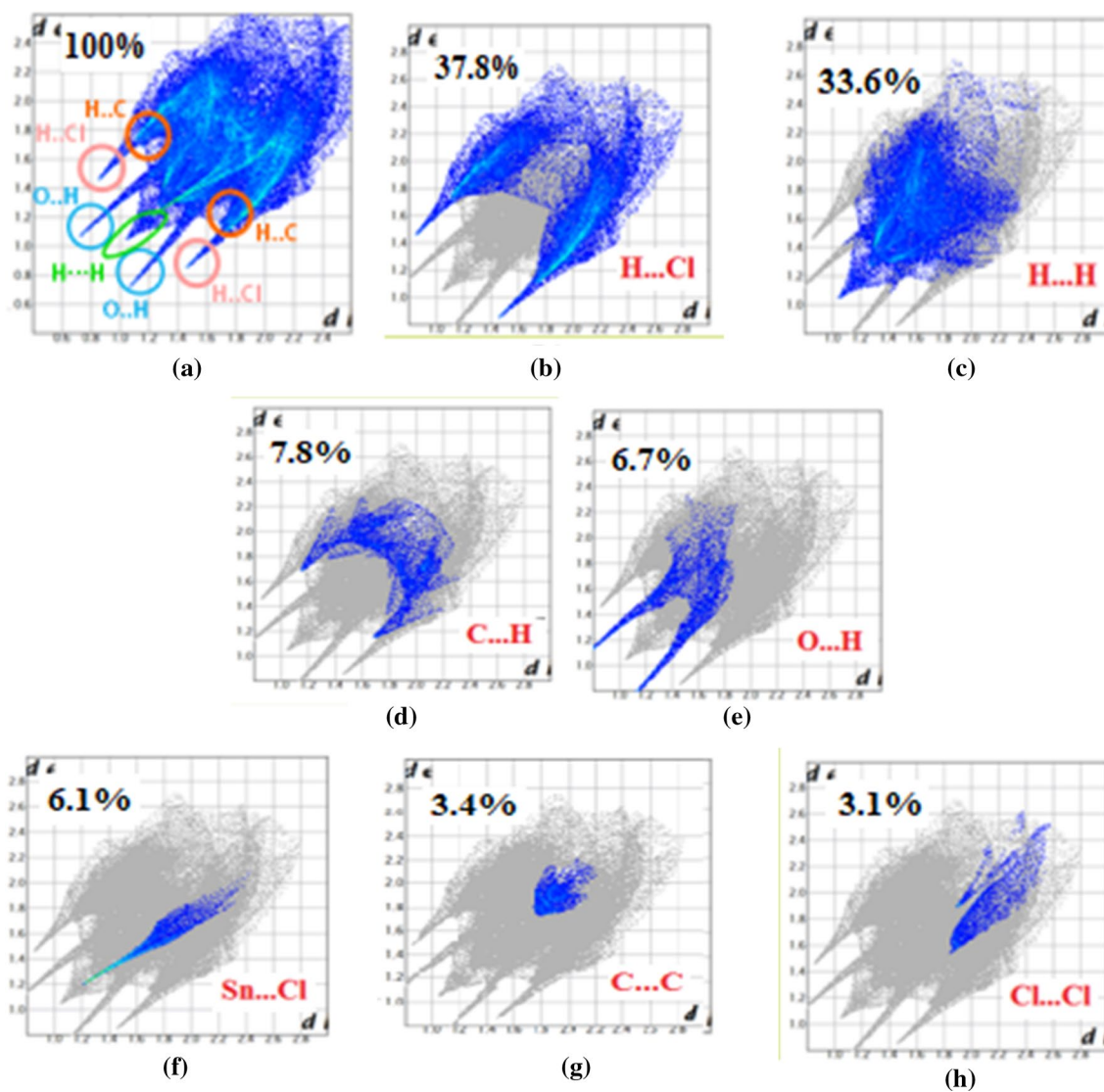


**Fig. 6** 2D fingerprint plot for  $(C_8H_{12}N)_2SnCl_6 \cdot 2H_2O$  showing the contribution from different contacts

**Table 4** Hirshfeld contact surface and enrichment ratios for  $(C_8H_{12}N)_2SnCl_6 \cdot 2H_2O$

Atoms	H	C	Cl	Sn	O	N
Surface %	59.75	7.3	25.05	3.05	3.35	0
H	0.941	–	–	–	–	–
C	0.894	6.38	0	0	0	–
O	1.674	0	0	0	0	–
Cl	1.263	0	0.494	–	0	–
Sn	0	0	3.99	0	0	–
N	–	–	–	–	–	–

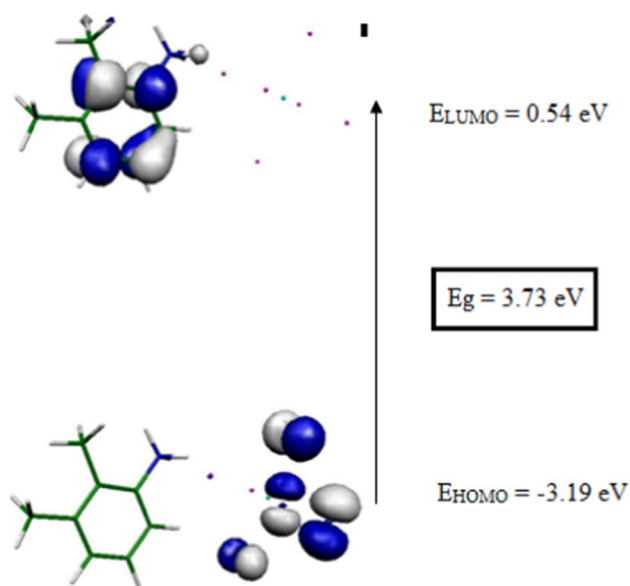


Fig. 7 Frontier orbitals in  $(C_8H_{12}N)_2SnCl_6 \cdot 2H_2O$

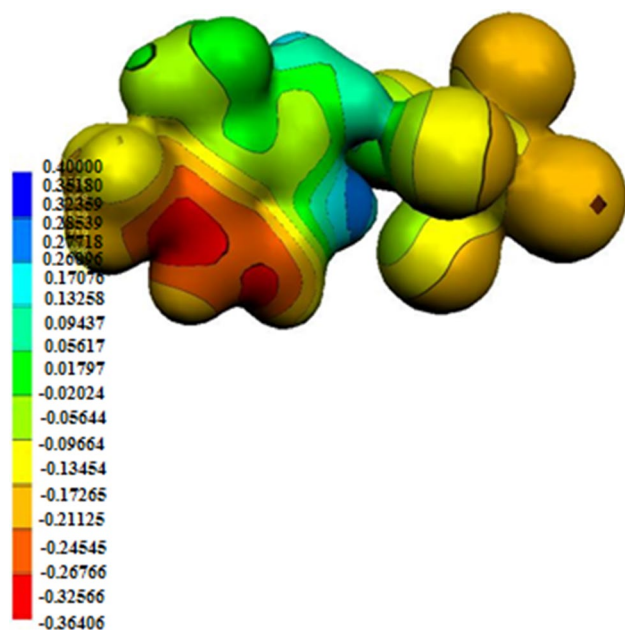
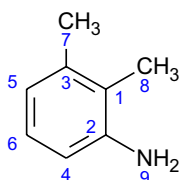


Fig. 8 MEP surface of  $(C_8H_{12}N)_2SnCl_6 \cdot 2H_2O$



For the anionic part of  $(C_8H_{12}N)_2SnCl_6 \cdot 2H_2O$ , the atomic charge distribution appears that the tin ion has a positive

charge of 1.103346, whereas the Cl atoms have negative charges varying between  $-0.416832$  and  $-0.512325$ . For the organic entity, the nitrogen atom has a negative charge of  $-0.932921$ . The C2 and C4 atoms have a negative charge, while the other six have positive charges. All the hydrogen atoms carry a positive charge. It is worth noting that the presence of the anion greatly alters the charge distribution of Mulliken on the aromatic group by polarizing it.

### Infrared spectral studies

To provide more information about the crystal structure, we have studied the vibrational properties of  $(C_8H_{12}N)_2SnCl_6 \cdot 2H_2O$  by FT-IR spectroscopy. To defeat the difficulties experienced inside the assignment of the observed bands, the experimental IR frequencies were compared to those calculated by the above DFT method with a tentative assignment of the observed bands. Bibliographic results on similar compounds were used to identify and interpret the band's characteristic of the functional groups shown within the compound (Guidara et al. 2014; Khemiri et al. 2008; Hrizi et al. 2012).

As it can be seen in Fig. 9 the two observed bands at  $3608$  and  $3540$   $cm^{-1}$  are allocated to the valence vibration  $\nu_{(O-H)}$  of  $H_2O$  molecules of crystallization. The DFT computations estimate the frequency of these bands at  $3863$  and  $3755$   $cm^{-1}$ . The group of bands located in the range

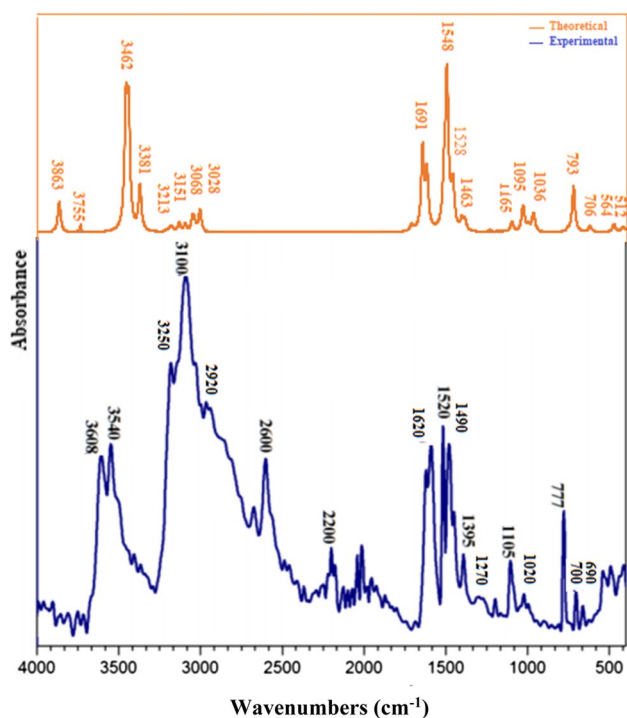
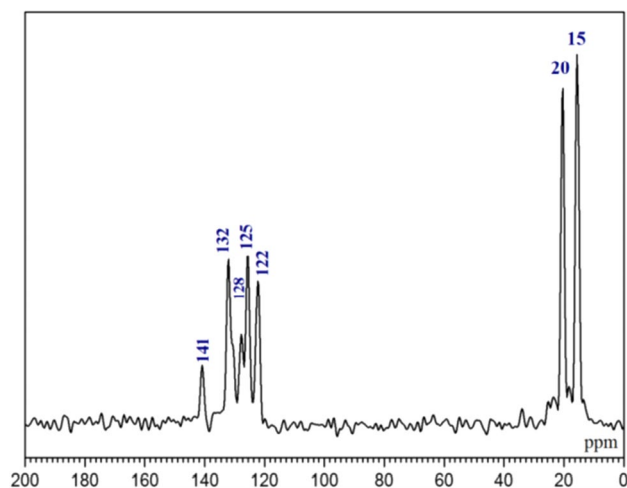


Fig. 9 Experimental and calculated infrared spectra of  $(C_8H_{12}N)_2SnCl_6 \cdot 2H_2O$



3200–2600  $\text{cm}^{-1}$  is related to the symmetrical and asymmetrical valence vibrations of ( $\text{NH}_3^+$ ), ( $\text{CH}_3$ ) and ( $\text{CH}$ ) groups. The bands at 3250 and 3100  $\text{cm}^{-1}$  correspond to the stretching vibration of N–H groups, the equivalent bands for this mode were found at 3462 and 3381  $\text{cm}^{-1}$ , respectively. The bands within 2920–2000  $\text{cm}^{-1}$  have been assigned to the C–H stretching bands and are predicted between 3212 and 3.28  $\text{cm}^{-1}$  by DFT calculation. The band situated at 1620  $\text{cm}^{-1}$  is assigned to the N–H deformation vibrations. This vibration is well observed by DFT calculations at 1691  $\text{cm}^{-1}$ . However, the band situated at 1520  $\text{cm}^{-1}$  corresponds to the water molecule's deformation vibration. The DFT estimates this mode at 1548  $\text{cm}^{-1}$ . As this structure contains various hydrogen bonds, these latter can impact the frequency as well as the intensity of these vibrations. The remaining bands, located below 1500  $\text{cm}^{-1}$ , are assigned to the out of plane deformation vibrations. The two bands at 1490  $\text{cm}^{-1}$  and 1395  $\text{cm}^{-1}$  are assigned to  $\nu_{(\text{C}=\text{C})\text{Ar}}$ . The DFT calculations predict this bands at 1528 and 1463  $\text{cm}^{-1}$  while the observed vibrations in the range 1020 and 1270  $\text{cm}^{-1}$  are allocated to the symmetric and asymmetric binding vibrations of C–C and  $\text{CH}_3$  additionally the valence vibration  $\nu_{(\text{C}-\text{N})}$ . The DFT estimates these modes between 1165 and 1036  $\text{cm}^{-1}$ . In addition, the existence of three bands around 777, 700 and 690  $\text{cm}^{-1}$  shows that the aromatic cycle is 1,2,3-trisubstituted, in agreement with the presence of the 2,3-dimethylanilinium cation in this compound.

The difference between the experimental spectrum and the calculated spectrum is because the theoretical spectrum has been recorded for the isolated molecules of the compound. Nevertheless, a close agreement is mostly accomplished in the fingerprint region as shown in Fig. S5 ( $R^2 = 0.9949$ ).



**Fig. 10** CP-MAS  $^{13}\text{C}$  NMR spectrum of  $(\text{C}_8\text{H}_{12}\text{N})_2\text{SnCl}_6 \cdot 2\text{H}_2\text{O}$

## CP-MAS $^{13}\text{C}$ NMR spectroscopy

Figure 10 displays the title compound's CP-MAS  $^{13}\text{C}$  NMR spectrum. The two peaks located at 15 and 20 ppm correspond to the carbon atoms of the two methyl groups grafted onto the aromatic ring of the organic cation 2,3-dimethylanilinium. Concerning the highest shift values between 122 and 141 ppm, the spectrum contains five peaks, in which the peak at 132 ppm is large and asymmetric (contains a shoulder). This spectrum can hence be interpreted as containing six peaks in this range corresponding to the six crystallographically independent aromatic carbon sites. This further confirms the presence of a single organic entity in the asymmetric unit. Moreover, the DFT calculations were attempted to assign the NMR resonance to the diverse crystallographic non-equivalent C atoms. The calculated chemical shifts, after optimization of proton positions, are given for TMS ( $d_{\text{abs}} = 190.8$  ppm). The results are presented in Table S2, showing a good agreement. However, the discrepancy between the calculated and the experimental values is mainly due to the fact that the molecule was taken in the isolated state ( $R^2 = 0.9941$ , Fig. S6).

## UV–Visible study

Figure 11 displays the experimental UV–Vis absorption spectrum recorded at room temperature. Figure 12c represents the calculated spectrum (Fig. 12a displays the spectrum of the organic cation alone and Fig. 12b displays the spectrum of the hexachlorostannate anions) and shows three bands. The first intense one at 257 nm, in agreement with the band observed experimentally at 250 nm, is related to the metal–ligand transition  $\text{Sn} \rightarrow \text{Cl}$  (MLCT) as it is observed in the calculated spectrum of the anion

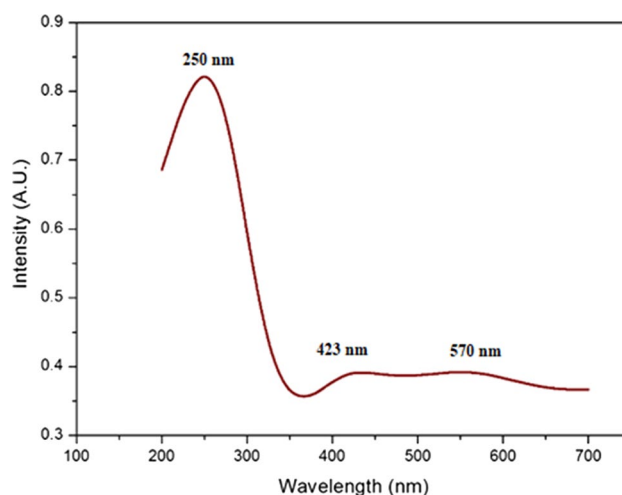


**Fig. 11** Experimental UV–visible absorption spectrum of  $(\text{C}_8\text{H}_{12}\text{N})_2\text{SnCl}_6 \cdot 2\text{H}_2\text{O}$

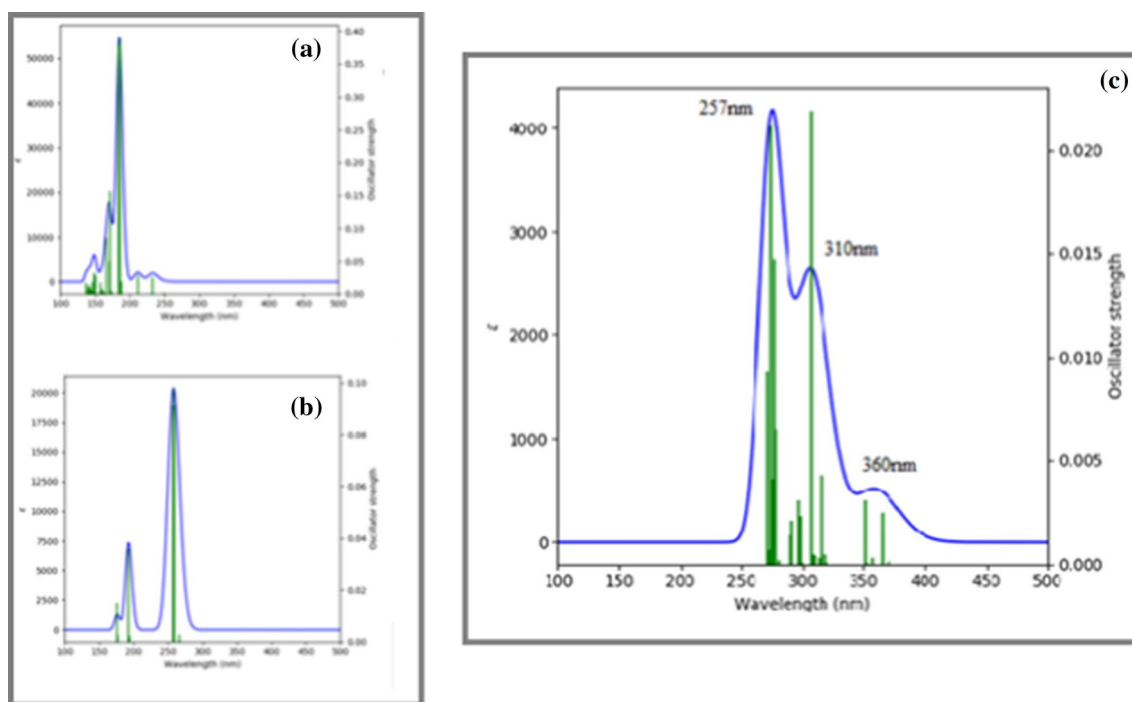


**Fig. 12** Calculated UV–visible spectrum of the organic entity alone (a), the inorganic entity alone (b) and the organic cation + inorganic anions in  $(C_8H_{12}N)_2SnCl_6 \cdot 2H_2O$

alone (Fig. 12b). The two other bands around 310 and 360 nm, corresponding experimentally to the bands at 423 and 570 nm, are a result of anion-cation electron transfer (Kesentini et al. 2015; Beranek et al. 2008).

### Photoluminescence study

Studying its possible use as a light-emitting substance. The spectrum obtained at room temperature is given in Fig. 13.

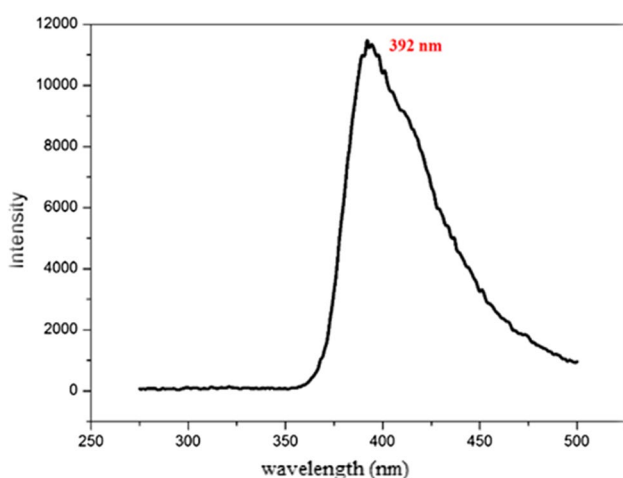


**Fig. 13** Photoluminescence spectrum of  $(C_8H_{12}N)_2SnCl_6 \cdot 2H_2O$

After excitation at  $\lambda = 250$  nm, the device detects one single emission, around 392 nm characteristic of the  $\pi \rightarrow \pi^*$  transition of the 2,3-dimethylanilinium cation (Welliemen et al. 1979).

### XPS analysis

The  $(C_8H_{12}N)_2SnCl_6 \cdot 2H_2O$  compound was also studied by XPS. The resulting spectrum is shown in Fig. 14. Each peak corresponds to bond energy which is specific to each element and shows the presence of carbon, chloride, nitrogen and tin. The main peaks are Cl 2p, Cl s, N 1s, Sn 3d, O 1s and are centered at 197.55, 285.8, 402.1, 486.33 and 532.46 eV, respectively. The profile due to the signals from Sn 3d highlights the presence of two peaks relating to tin Sn  $3d_{3/2}$  (~495.3 eV) and Sn  $3d_{5/2}$  (~487.1 eV). This last peak corresponds to the oxidation state (IV). Moreover, the examination of C 1s peaks shows the presence of two peaks located at 285 eV and 287.2 eV confirms the nature of the bonds established by the carbon atoms in this compound. In fact, the most intense peaks located at 285 eV are attributed to the C–C bond while the low-intensity peak observed at 287.2 eV is attributed to the carbon bonded to nitrogen. A single weak observed at 401.7 eV on the deconvoluted XPS spectrum of nitrogen N 1s indicates the presence of the N–C bond in  $(C_8H_{12}N)_2SnCl_6 \cdot 2H_2O$ . These calculations are about to certify the valence sum of the title compound (Camalli et al. 1990).

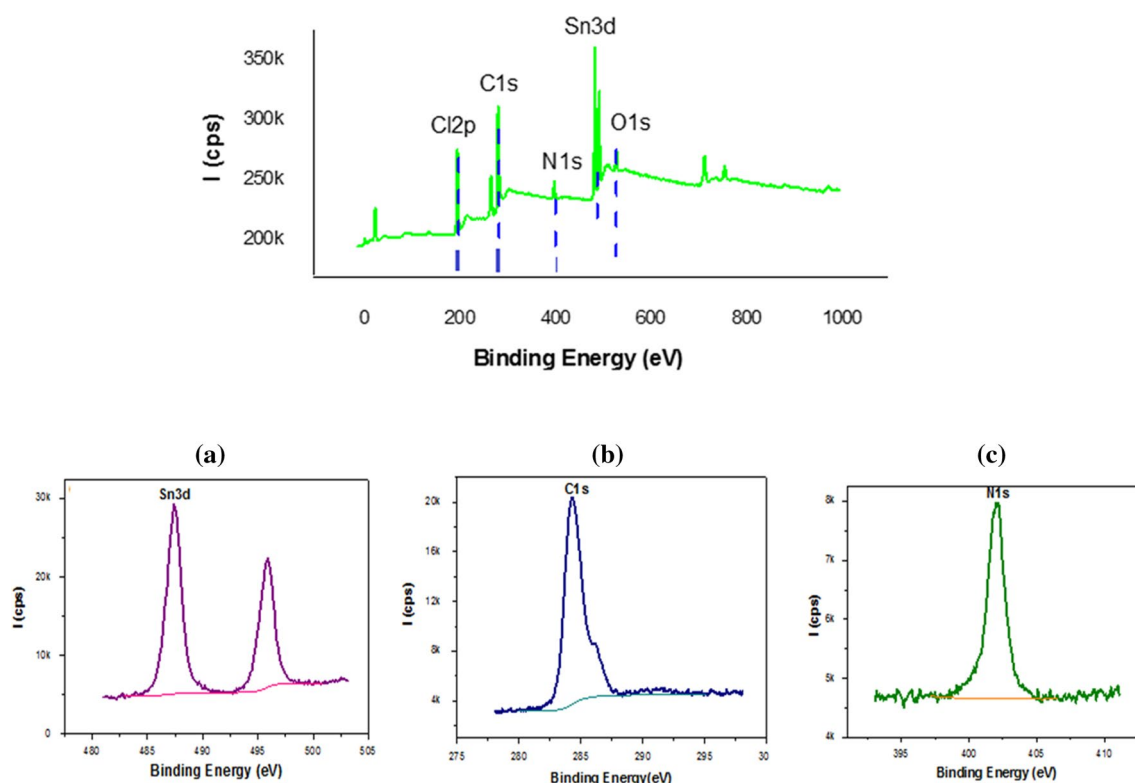


Fig. 14 XPS survey scan of  $(C_8H_{12}N)_2SnCl_6 \cdot 2H_2O$

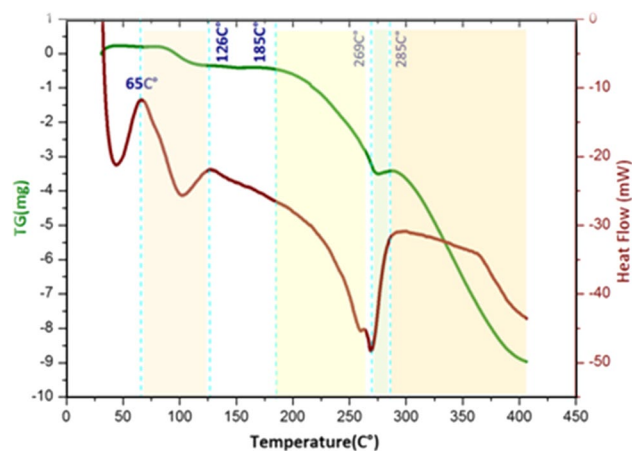


Fig. 15 TGA/DTA curves for  $(C_8H_{12}N)_2SnCl_6 \cdot 2H_2O$

## Thermal analysis

Figure 15 represents the results from DTA/TGA analyzing. The thermogram shows that the first broad endothermic peak around 102 °C can be related to the first stage of the dehydration of the sample, as the mass loss represented by this

peak is equal to 0.58 mg (5.22%) and corresponds well to the theoretical loss of mass relative to the departure of the water molecules ( $m_{theo} = 0.548$  mg, 4.95%). From 185 to 450 °C, the ATD curve presents a series of endothermic peaks, accompanied by an important mass loss. Indeed, the thermal decomposition of the anhydrous phase was carried out in several successive stages. First, the cation 2,3-dimethylanilinium begins to decompose in relatively rapid stages from 185 to 269 °C. Then, we observe the degradation and the release of chloride and the elimination of the tin complex.

## Conclusion

In summary, we have synthesized and investigated the crystal structure of a new compound. The obtained single-crystal structure was characterized by physico-chemical methods. The hybrid grows at room temperature and belongs to the triclinic system  $P\bar{1}$ . The purity of the compound is confirmed by PXRD. The stabilization in the crystal structure is provided by the establishment of N–H...Cl, N–H...O, O–H...O and O–H...Cl hydrogen bonds between the cations, the anions and the water molecule leading to a 3D network. The Hirshfeld surface study reveals the title compound's intermolecular contact percentage and verifies the existence of electrostatic interactions in the structure. Moreover, the

FT-IR and CP-MAS<sup>13</sup>C NMR spectra confirms the structure determined by XRD. The optical spectrum presents three absorption bands and the PL spectrum shows an intense fluorescence property. Additionally, the valence sum calculations are revealed by XPS examination results. Finally, the thermal analysis shows that the title compound remains stable up to 102 °C.

**Supplementary Information** The online version contains supplementary material available at <https://doi.org/10.1007/s11696-021-01974-4>.

**Acknowledgements** The authors extend their appreciation to the Deanship of Scientific Research at King Saud University for funding this work through Researchers Supporting Project number (RSP-2021-242).

## References

- Adhikari S, Kar T, Seth SK (2016) Synthesis, crystal growth and characterization of di-valine maleic—a new nonlinear optical material. *RSC Adv* 6:99139–99148. <https://doi.org/10.1039/C6RA21466E>
- Aloui Z, Valeria F, Abid S, Rzaigui M, Nasr CB (2015) Synthesis and Physico-chemical studies of a new non-centrosymmetric organic-inorganic hybrid material: [2,3-(CH<sub>3</sub>)<sub>2</sub>C<sub>6</sub>H<sub>3</sub>NH<sub>3</sub>]4BiBr6NO<sub>3</sub>·2H<sub>2</sub>O. *Chem Sci* 127(3):461–466. <https://doi.org/10.1007/s12039-015-0799-9>
- Amri O, Abid S, Rzaigui M (2008) Synthesis and crystal structure of 2, 6-xylidinium cyclohexaphosphate tetrahydrate. *Anal Sci* 24:277–278. <https://doi.org/10.2116/analsci.24.x277>
- Baur WH (1974) Rutile-type compounds. V. refinement of MnO<sub>2</sub> and MgF<sub>2</sub>. *Acta Crystallogr B* 32:2200–2204. <https://doi.org/10.1107/S0567740876007371>
- Beranek R, Kisch H (2008) Tuning the optical and photoelectrochemical properties of surface-modified TiO<sub>2</sub>. *Photochem Photobiol* 7:40–48. <https://doi.org/10.1080/1042650070141839810.1039/B711658F>
- Blessing RH (1995) An empirical correction for absorption anisotropy. *Acta Crystallogr Sect A* 51:33–38. <https://doi.org/10.1107/S0108767394005726>
- Brandenburg K (1998) Diamond version 2.0 impact Gbr, Bonn, Germany
- Bujak M, Zaleski J (2001) High temperature ferro-paraelectric phase transition in tris (trimethylammonium) nonachlorodiantimonate (III)(TMACA) studied by X-ray diffraction method. *Cryst Eng* 4:241–252. [https://doi.org/10.1016/S1463-0184\(01\)00018-1](https://doi.org/10.1016/S1463-0184(01)00018-1)
- Camalli M, Caruso F, Mattogno G, Rivarola E (1990) Adducts of tin (IV) and organotin (IV) derivatives with 2, 2'-azopyridine II. Crystal and molecular structure of SnMe<sub>2</sub>Br 2AZP and further mössbauer and photoelectronic spectroscopic studies. *Inorg Chim Acta* 170:225–231. [https://doi.org/10.1016/S0020-1693\(00\)80479-X](https://doi.org/10.1016/S0020-1693(00)80479-X)
- Chouaib H, Kamoun S, Costa LC, Graça MPF (2015) Synthesis, crystal structure and electrical properties of N, N-dimethylanilinium trichloridostannate (II). *J Mol Struct* 1102:71–80. <https://doi.org/10.1016/j.molstruc.2015.08.041>
- Chouaib H, Elfaleh N, Karoui S, Kamoun S, Graça MPF (2016) Synthesis, crystal structure, thermal analysis and dielectric properties of (C<sub>8</sub>H<sub>12</sub>N)<sub>3</sub> SnCl<sub>6</sub> Cl compound. *J Synth Met* 217:129–137. <https://doi.org/10.1016/j.synthmet.2016.03.029>
- Era M, Morimoto S, Tsutsui T, Saito S (1994) Organic-inorganic heterostructure electroluminescent device using a layered perovskite semiconductor (C<sub>6</sub>H<sub>5</sub>C<sub>2</sub>H<sub>4</sub>NH<sub>3</sub>)<sub>2</sub>PbI<sub>4</sub>. *Appl Phys Lett* 65:676–678. <https://doi.org/10.1063/1.112265>
- Farrugia LJ (1999) WinGX suite for small-molecule single-crystal crystallography. *J Appl Cryst* 32:837–838. <https://doi.org/10.1107/S0021889899006020>
- Feddaoui I, Abdelbaky MS, García-Granda S, Essalah K, Nasr CB, Mrad ML (2019) Synthesis, crystal structure, vibrational spectroscopy, DFT, optical study and thermal analysis of a new stannate (IV) complex based on 2-ethyl-6-methylanilinium (C<sub>9</sub>H<sub>14</sub>N)<sub>2</sub>[SnCl<sub>6</sub>]. *J Mol Struct* 1186:31–38. <https://doi.org/10.1016/j.molstruc.2019.03.009>
- Fonseca TL, De Oliveira HCB, Amaral OAV, Castro MA (2005) MP2 static first hyperpolarizability of azo-enaminone isomers. *Chem Phys Lett* 413:356–361. <https://doi.org/10.1016/j.cplett.2005.08.007>
- Guidara S, Ahmed AB, Abid Y, Feki H (2014) Molecular structure, vibrational spectra and nonlinear optical properties of 2,5-dimethylanilinium chloride monohydrate: a density functional theory approach. *J Spectro Chim Acta Part A* 127:275–285. <https://doi.org/10.1016/j.saa.2014.02.028>
- Hajlaoui S, Chaabane I, Oueslati A, Guidara K (2013) Anomalous dielectric behavior in centrosymmetric organic-inorganic hybrid bis-tetrapropylammoniumhexachlorostannate. *Crystal structure and properties. Solid State Sci* 25:134–142. <https://doi.org/10.1016/j.solidstatesciences.2013.09.004>
- Hrizi C, Chaari N, Abid Y, Chniba-Boudjada N, Chaabouni S (2012) Structural characterization, vibrational and optical properties of a novel one-dimensional organic-inorganic hybrid based-iodobismuthate (III) material, [C<sub>10</sub>H<sub>7</sub>NH<sub>3</sub>]BiI<sub>4</sub>. *Polyhedron* 46:41–46. <https://doi.org/10.1016/j.poly.2012.07.062>
- Kagan CR, Mitzi DB, Dimitrakopoulos CD (1999) Organic-inorganic hybrid materials as semiconducting channels in thin-film field-effect transistors. *Science* 286:945–947. <https://doi.org/10.1126/science.286.5441.945>
- Karoui K, Rhaïem AB, Guidara K (2012) Dielectric properties and relaxation behavior of [TMA]<sub>2</sub>Zn<sub>0.5</sub>Cu<sub>0.5</sub>Cl<sub>4</sub> compound. *Phys B* 407:489–493. <https://doi.org/10.1016/j.physb.2011.11.021>
- Kessentini A, Belhouchet M, Suñol JJ, Abid Y, Mhiri T (2015) Crystal structure, vibrational studies and optical properties of a new organic-inorganic hybrid compound (C<sub>10</sub>H<sub>28</sub>N<sub>4</sub>) CuCl<sub>5</sub>Cl·4H<sub>2</sub>O. *Spectro Chim Acta* 134:28–33. <https://doi.org/10.1016/j.saa.2014.06.073>
- Khanam H, Mashrai A, Siddiqui N, Ahmad M, Alam MJ, Ahmad S (2015) Structural elucidation, density functional calculations and contribution of intermolecular interactions in cholest-4-en-3-one crystals: Insights from X-ray and Hirshfeld surface analysis. *J Mol Struct* 1084:274–283. <https://doi.org/10.1016/j.molstruc.2014.12.027>
- Khemiri H, Nasr CB, Rzaigui M, Brahim K (2008) Crystal structure, <sup>31</sup>P, <sup>13</sup>C MAS-NMR, IR spectroscopy and thermal investigations of 2, 6-dimethylanilinium dihydrogenmonophosphate monohydrate. *J Phosphorus, Sulfur, Silicon* 182:2269–2282. <https://doi.org/10.1080/10426500701418398>
- Kumar SM, Manjunath BC, Lingaraju GS, Abdoh MMM, Sadashiva MP, Lokanath NK (2013) A Hirshfeld surface analysis and crystal structure of 2-[1-(2-Fluoro-Phenyl)-1H-tetrazol-5-YI]-4-Methoxy-Biphenyl-2-Carbaldehyde. *Cryst Struct Theory Appl* 2:37258. <https://doi.org/10.4236/csta.2013.23017>
- Ma YH, Ge SW, Wang W, Sun BW (2015) Studies on the synthesis, structural characterization, Hirshfeld analysis and stability of apovincamine (API) and its co-crystal (terephthalic acid: Apovincamine = 1: 2). *J Mol Struct* 1097:87–97. <https://doi.org/10.1016/j.molstruc.2015.05.014>
- Macrae CF, Edgington PR, McCabe P, Pidcock E, Shields GP, Taylor R, Streek JVD (2006) Mercury: visualization and analysis of

- crystal structures. *J Appl Cryst* 39:453–457. <https://doi.org/10.1107/S002188980600731X>
- Masternak J, Zienkiewicz-Machnik M, Kowalik M, Jabłońska-Wawrzycka A, Rogala P, Adach A, Barszcz B (2016) Recent advances in coordination chemistry of metal complexes based on nitrogen heteroaromatic alcohols. Synthesis, structures and potential applications. *Coord Chem Rev* 327:242–270. <https://doi.org/10.1016/j.ccr.2016.01.007>
- Mathlouthi M, Valkonen A, Rzaigui M, Smirani W (2017) Structural characterization, spectroscopic, thermal, AC conductivity and dielectric properties and antimicrobial studies of  $(C_8H_{12}N)_2[SnCl_6]$ . *Phase Trans* 90:399–414. <https://doi.org/10.1080/01411594.2016.1212194>
- McKinnon JJ, Spackman MA, Mitchell AS (2004) Novel tools for visualizing and exploring intermolecular interactions in molecular crystals. *Acta Crystallogr Sect B* 60:627–668. <https://doi.org/10.1107/S0108768104020300>
- Mrad ML, Belhajsalah S, Abdelbaky MSM, García-Granda S, Essalah K, Ben Nasr C (2019) Synthesis, crystal structure, vibrational, optical properties, and a theoretical study of a new Pb (II) complex with bis (1-methylpiperazine-1, 4-dium): $[C_5H_{14}N_2]_2PbCl_6 \cdot 3H_2O$ . *J Coord Chem* 72:358–371. <https://doi.org/10.1080/00958972.2018.1562177>
- Ouerghi Z, Roisnel T, Fezai R, Kefi R (2018) Physico-chemical characterization, Hirshfeld surface analysis and opto-electric properties of a new hybrid material: tris (2-amino-5-chloropyridinium) hexachlorobismuthate (III). *J Mol Struct* 1173:439–447. <https://doi.org/10.1016/j.molstruc.2018.05.084>
- Płowaś I, Szklarz P, Jakubas R, Bator G (2011) Structural, thermal and dielectric studies on the novel solution grown (4-dimethylaminopyridinium) chloroantimonate (III) and chlorobismuthate (III) crystals. *Mater Res Bull* 46:1177–1185. <https://doi.org/10.1016/j.materresbull.2011.04.013>
- Pradeesh K, Agarwal M, Rao KK, Prakash GV (2010) Synthesis, crystal structure and optical properties of quasi-one-dimensional lead (II) iodide:  $C_{14}H_{18}N_2Pb_2I_6$ . *Solid State Sci* 12:95–98. <https://doi.org/10.1016/j.solidstatesciences.2009.10.011>
- Ringer AL, Figgs MS, Sinnokrot MO, Sherrill CD (2006) Aliphatic C–H/ $\pi$  interactions: methane–benzene, methane–phenol, and methane–indole complexes. *J Phys Chem A* 110:10822–10828. <https://doi.org/10.1021/jp062740l>
- Saber Lassoued M, Abdelbaky MS, Lassoued A, Mendoza-Meroño R, Ammar S, Gadri A, Ben Salah A, García-Granda S (2017) Synthesis, crystal structure, vibrational spectroscopy and photoluminescence of new hybrid compound containing chlorate anions of stanate (II). *J Mol Struct* 1141:660–667. <https://doi.org/10.1016/j.molstruc.2017.03.124>
- Shahzadi S, Khan HN, Ali S, Helliwell M (2008) Bis (4-methylpiperidinium) hexachloridostannate (IV). *Acta Cryst E* 64:573–573. <https://doi.org/10.1107/S1600536808007368>
- Sheldrick GM (1997) SHELXL97, Program for crystal structure refinement. University of Gottingen, Germany
- Sheldrick GM (2008) A short history of SHELX. *Acta Crystallogr Sect A* 64:112–122. <https://doi.org/10.1107/S0108767307043930>
- Smirani W, Rzaigui M (2009) Crystalline and molecular structure of hydrated 2,6-xylylidinium tetrachlorozincate (II). *J Chem* 6:569–576. <https://doi.org/10.1155/2009/836238>
- Spackman MA, Jayatilaka D (2009) Hirshfeld surface analysis. *Cryst Eng Comm* 11:19–32. <https://doi.org/10.1080/1042650070141839810.1039/B818330A>
- Turner MJ, McKinnon JJ, Wolff SK (2017) CrystalExplorer17.5. University of Western Australia, Perth
- Vaschetto ME, Retamal BA, Monkman AP, Springborg M (1999) First-principles calculations of pyridines: from monomer to polymer. *J Phys Chem A* 103:11096–11103. <https://doi.org/10.1021/jp992204b>
- Visbal R, Gimeno MC (2014) N-heterocyclic carbene metal complexes: photoluminescence and applications. *Chem Soc Rev* 43:3551–3574. <https://doi.org/10.1039/C3CS60466G>
- Vishwakarma AK, Ghalsasi PS, Navamoney A, LanY PAK (2011) Structural phase transition and magnetic properties of layered organic–inorganic hybrid compounds: p-Haloaniliniumtetrachlorocuparate (II). *Polyhedron* 30:1565–1570. <https://doi.org/10.1016/j.poly.2011.03.025>
- Willems H, Van De Vondel DF, Van Der Kelen GP (1979) An ESCA study of tin compounds. *InorgChimActa* 34:175–180. [https://doi.org/10.1016/S0020-1693\(00\)94698-X](https://doi.org/10.1016/S0020-1693(00)94698-X)
- Zdanowska-Frączek M, Hołderna-Natkaniec K, Frączek ZJ, Jakubas R (2009) Molecular dynamics and electrical conductivity of  $(C_3N_2H_5)_3Bi_2Cl_{11}$ . *Solid State Ionics* 180:9–12. <https://doi.org/10.1016/j.ssi.2008.10.018>

**Publisher's Note** Springer Nature remains neutral with regard to jurisdictional claims in published maps and institutional affiliations.